

Article

Energy Utilization and Carbon Reduction Potential of Solar Energy in Residential Blocks: A Case Study on a Tropical High-Density City in China

Jingtao Li ^{1,2}, Zhixin Li ^{3,*}, Yao Wang ¹ and Hong Zhang ^{3,*}

¹ Academy of Arts & Design, Tsinghua University, Beijing 100190, China; li-jt22@mails.tsinghua.edu.cn (J.L.); wangyao22@mails.tsinghua.edu.cn (Y.W.)

² School of Art, Hubei University, Wuhan 430061, China

³ School of Architecture, Tsinghua University, Beijing 100190, China

* Correspondence: lizhixin22@mails.tsinghua.edu.cn (Z.L.); zhanghong@tsinghua.edu.cn (H.Z.)

Abstract: Energy efficiency in high-density urban areas is increasingly gaining more attention as the energy crisis and environmental issues worsen. Urban morphology is an essential factor affecting the energy consumption and solar energy development potential of buildings. In response to the research gap of previous studies that only analyzed building energy consumption or solar energy potential from a single objective, this paper aims to combine the two objectives of block-scale building energy consumption and solar development potential to explore the joint influence of urban residential morphological elements on correlations between the two. By investigating and summarizing 100 sample cases of Wuhan city blocks, 30 urban residential block prototypes were constructed. The correlations between the leading morphological indicators of the blocks with the building energy consumption and solar energy potential of the residential prototypes were quantified, respectively. The study results show that at certain floor area ratios, the highest solar power generation can be achieved with a mixture of high-rise slabs and high-rise towers, but the building energy intensity level is relatively high; combining building energy consumption and solar power generation, the residential block form of high-rise towers and low-rise villas has incredible energy-saving potential. In addition, the regression analysis results show that three block form indicators, namely the roof-to-envelope area ratio, compactness, and site coverage, have the most prominent influence on building energy intensity and solar power generation, and they all show positive correlations. This study can provide suggestions for urban residential planners and managers to promote urban energy conservation at the design stage.

Keywords: urban form; PV potential; building energy consumption; parametric study; carbon emissions



Citation: Li, J.; Li, Z.; Wang, Y.; Zhang, H. Energy Utilization and Carbon Reduction Potential of Solar Energy in Residential Blocks: A Case Study on a Tropical High-Density City in China. *Sustainability* **2023**, *15*, 12975. <https://doi.org/10.3390/su151712975>

Academic Editors: Jianghua Wang and Bin Yang

Received: 19 July 2023

Revised: 20 August 2023

Accepted: 23 August 2023

Published: 28 August 2023



Copyright: © 2023 by the authors. Licensee MDPI, Basel, Switzerland. This article is an open access article distributed under the terms and conditions of the Creative Commons Attribution (CC BY) license (<https://creativecommons.org/licenses/by/4.0/>).

1. Background

Cities are facing a severe energy crisis and environmental problems, which are the primary causes of excessive energy consumption and CO₂ emissions [1–3]. According to the latest report of IPCC [4], 3.3 billion people will be significantly affected by environmental degradation by 2050. Governments and scholars have made ongoing efforts to reduce energy use while enhancing renewable energy development [5,6]. PVSITES [7], MUSTEC [8], BIOSOL [9], and other projects organized and carried out by the European Union, among others, aim to enhance the development of solar energy resources and thus achieve sustainable urban development through renewable energy projects. To achieve energy conservation and emission reduction, China has committed to reaching peak carbon emissions by 2030 or earlier and plans to increase non-fossil energy sources to 20%, of which solar power will be promoted as a priority [10]. The development of sustainable cities will be further promoted by reducing energy consumption and increasing the effectiveness of solar energy resource exploitation.

Urban settlements show excellent potential and numerous advantages in energy savings and solar resource development [11,12]. Residential buildings, which are the most significant and numerous building type in cities, have a variety of energy types and enormous scope for energy savings [13]. At the same time, the flat roofs and large building façades of residential buildings offer more possibilities for developing solar energy resources. Solar energy resource development is receiving more attention in promoting the planning and construction of zero-energy settlements. How to fully enhance the potential of solar energy resources while reducing building energy use is of great significance for improving overall energy use efficiency and guiding the planning and design of settlements.

2. Literature Review

2.1. Research on Energy Savings in Urban Settlements

As revealed by the existing studies on energy consumption in urban settlements, residential neighborhoods have significant potential for energy savings. In a study on energy consumption in urban dwellings in warm and humid climates, Muhammad Abdul Mujeebu et al. [14] found that the energy performance index (EPI) of buildings could be reduced by 63.5% by using active energy efficiency measures (EEMs), such as air conditioning and lighting control, in the building design phase. In addition, Ana Paola Vargas et al. [15] studied the impact of passive retrofit design strategies on building energy consumption for urban housing in the Mexican region. It was found that the passive design strategy achieved a maximum total emission reduction of 23.5%, with a payback period of 5.8 years. In Hong Kong, using Energy Plus, S. Liu et al. [16] found that an overall passive design was able to reduce the annual cooling energy consumption of residential buildings by 56.7% in simulations, and analysis of different passive design strategies provided a good guide for residential energy efficiency design. F.A. Chi et al. [17] simulated residential energy efficiency strategies. After analyzing and evaluating the effectiveness of implementation and the residential energy use behavior in China, they concluded that energy consumption could be saved by 39% through passive design and planning methods. Zhou et al. [18] explored heating energy consumption in buildings in northern China by involving and optimizing the operation process of the residential building envelope. They obtained a heating energy-saving potential of 30.9–66.1% for the envelope in Chinese residential buildings. The research above shows that residential buildings have immense potential for energy savings and are worthy of attention.

Urban morphology has a significant impact on building energy consumption. The geometric form and layout form of buildings in a city can directly affect the overall building energy intensity within a block, such as the length, width, and height of buildings, as well as urban form elements, such as enclosed or open layouts [19]. Sundus Shareef [20] explored the effect of urban form on building cooling energy consumption for the local climatic conditions in the UAE, and the study results manifested that orientation change was the most significant influencing factor. Y. Shi et al. [21] analyzed the correlation between hospital building layout and energy consumption by surveying 30 hospitals. They found that “L” shaped buildings had the best energy-saving potential among the three main hospital building layouts, with an energy-saving rate of 3.5%. Ahmadian et al. [22] analyzed the effects of pavilions, terraces, courts, and tunnel courts on the energy use intensity of four building layouts using a prototype construction. X. X. Xie et al. [23] explored the influence of the local microclimate on building energy consumption under different building forms, and the results proved that differences in building forms could lead to annual heating energy intensity variations of 1.1–7.3%. From the above studies, it can be seen that urban morphological changes have a significant impact on building energy storage.

2.2. Study of Solar Energy Utilization in Urban Settlements

Solar resources should be exploited based on an accurate assessment of the solar potential. Many sophisticated tools and software, such as GIS and parametric techniques,

enable scientific calculation of solar resource potential. Juan José Sarralde et al. [24] explored the solar potential in urban residential areas of London using GIS and Python scripts and evaluated the solar radiation potential of building roofs and façades by modeling 4718 urban settlement examples. Daniele Groppi et al. [25] used GIS tools to quantify the building energy consumption and solar potential in urban areas. They found enormous potential for solar energy development in residential buildings in both historic and new urban areas. Z. Q. Chen et al. [26] precisely evaluated the solar radiation intensity and the total area of building roofs within the city, using Shanghai as an example, and pointed out the great potential for gain from solar resource exploitation. It has been demonstrated that solar energy resources are abundant in cities and have great potential for solar energy resource development. Yawning An et al. [27] used GIS software to model and analyze the solar energy potential of four representative areas in Shenzhen. The analysis results showed that Shenzhen had vast solar potential, with 92% of the building rooftops producing more than 1000 kWh/m² per year, which provided an alternative energy source for residential and local electricity consumption in Shenzhen. Deniz Yildirim et al. [28] calculated and verified the rooftop solar potential of Istanbul using solar, atmospheric, and LiDAR data for measurements. It was finally found that Istanbul's total rooftop power generation could meet 67% of the city's total electricity consumption in 2019. The current studies have indicated abundant solar energy reserves in cities, and scientific utilization and exploitation of solar energy resource potential will significantly benefit urban energy conservation.

In high-density cities, mutual shading between buildings can significantly impact the potential of solar resource exploitation. The study of solar resource potential from the perspective of urban form has become a pressing issue in this field. Akshay Kaleshwarwar et al. [29] evaluated the solar potential under five different urban building forms (UBFs) in Nagpur, India, from the perspective of urban form. They found that site coverage, roof area, and building density were the key indicators that determined the urban building form. J. J. Li et al. [30] analyzed the impact of different urban form indicators on solar potential by constructing a prototype urban block, reporting that building density was the most crucial indicator affecting the development of solar resources. At the same time, U-shape and Court 1 types are the most promoted solar building forms. Using vernacular architecture, Z. M. Shi et al. evaluated the solar potential of 18 examples of dense urban blocks. They determined that the volume ratio was the most critical indicator affecting solar resource development, followed by site coverage and building pattern. On the other hand, Michele Morganti et al. [31] selected 14 examples of blocks in dense cities in the Mediterranean region. Seven morphological indicators of the examples were counted, such as density, floor area ratio, and average height, and the radiant values of the façades of the block examples were simulated. Through the correlation between morphological indicators and radiation values, the most significant indicators were density, façade-to-base area ratio, and sky factor. When studying the urban environment of Singapore, K.H. Poon et al. [32] concluded that the sky openness factor (SEF) and sky view factor (SVF) were most highly correlated with the radiant illuminance of roofs and façades of buildings by correlating 10 major morphological parameters in blocks with the development potential of solar energy resources. The study of the influence of urban morphology on solar energy exploitation potential demonstrates a close link between the two.

From the above studies, it can be found that changes in block morphology in the urban environment will have a collective impact on both building energy consumption and solar energy development potential; however, most of the existing studies only quantitatively assessed the energy-saving levels of residential communities from the perspective of a single indicator, which is not conducive to the planning and design of residential communities aiming at comprehensive energy savings. Therefore, it is necessary to consider the comprehensive impact of morphology on both aspects to realize their balanced correlation and improve the comprehensive energy-saving levels of residential communities. The problems in existing research are summarized as follows:

1. Insufficient research on comprehensive building energy efficiency-oriented urban settlements. Current research on the integrated energy consumption of urban neighborhoods taking into account their solar potential is mainly focused on office buildings and other types of public buildings, while research on the integrated energy consumption of neighborhoods in urban settlements with superimposed solar potential needs to be supplemented;
2. The current research on energy efficiency in blocks is only qualitative from the perspective of building energy consumption or solar energy development potential. The energy efficiency of urban blocks should be quantified at both open-source and low-cost levels, which will serve as a more practical basis for renewable energy development and block planning in urban residential blocks;
3. Lack of prototype research. The current research on the potential of solar energy development in urban blocks is mainly based on actual blocks as examples. The laws are objectively described from existing block morphological indicators. However, the laws should be more comprehensively and quantitatively analyzed from the perspective of urban block prototypes.

To solve the above problems, 100 actual urban blocks in Wuhan were investigated in this study, and based on the results, 30 prototypes of typical urban residential buildings in Wuhan were constructed. Then, using a block-scale building energy consumption simulation tool and the solar energy potential assessment method, the energy intensity and solar resource potential of the 30 settlement prototypes were evaluated, respectively. Finally, correlation and regression analyses were used to quantitatively analyze the relevance of urban residential district morphology on the impact of building energy intensity and solar energy potential, and comprehensive energy efficiency indicators were selected to quantitatively analyze the comprehensive energy-saving benefits of superimposed solar energy. The results can provide scientific guidance for the planning and construction of zero-energy residential blocks and the sustainable development of cities.

3. Methods

This paper aimed to find the optimal form of energy use in urban settlements, including both energy and electricity consumption and renewable energy use. Given this, a methodology for analyzing the energy-saving potential of urban settlements was constructed, and the study was carried out in five specific steps, as shown in Figure 1:

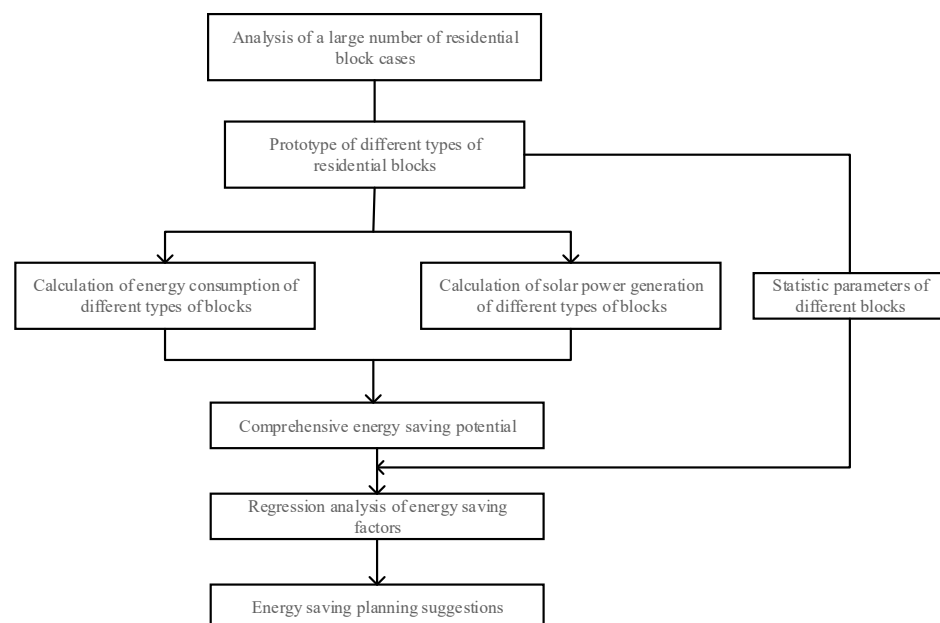


Figure 1. Five Steps of the Analysis Method for Energy-Saving Potential in Urban Residential Blocks.

Step 1: Real neighborhood sample data were obtained. This stage was used to obtain the multidimensional morphology of urban neighborhoods through field research, satellite maps, and streetscape images, and to classify neighborhoods according to their morphological type. The morphological parameter variables were controlled to build prototypes of different types of urban residential neighborhoods.

Step 2: The morphological parameters of different types of neighborhoods were counted according to the classification results of the residential neighborhood types.

Step 3: The building energy intensity data and solar power potential in each type of neighborhood were calculated and evaluated by software simulation.

Step 4: The correlations between the influences of morphological parameters of different types of neighborhoods on the building energy consumption and solar energy utilization potential in the neighborhood were calculated and analyzed, and a combined assessment of different types of residential neighborhood cases was carried out using the comprehensive energy-saving potential.

Step 5: Analysis was implemented and recommendations are provided for solar energy utilization and energy conservation in different block types based on the results of the calculations and analysis in Steps 3 and 4.

3.1. Subsection Selection of Urban Residential Neighborhood Types

In this study, the residential neighborhoods of Wuhan, a typical high-density city in the hot summer and cold winter region of China, were taken as examples. Wuhan is a typical high-density city in China and the construction of residential neighborhoods has been rising year by year due to its large population, presenting a large number of neighborhood types with rich morphologies. The basic unit of this study was the urban neighborhood, which is the smallest area surrounded by external roads in urban planning, usually subdivided into smaller parcels, as a basic component of the urban structure. Urban residential neighborhoods mainly consist of residential buildings of similar types in terms of form, function, and spatial correlation.

First, the residential neighborhoods within the third ring road of Wuhan were screened using web-based, open-source data, and a sample of about 100 residential neighborhoods established within the last 15 years was selected (Figure 2). The screened 100 samples were spatially distributed in Wuhan in a regular pattern and involved several areas of the city, such as Jiangan District, Qiaokou District, Wuchang District, Hongshan District, Qingshan District, and Hanyang District, which basically represented the general condition of contemporary residential neighborhoods in Wuhan in terms of architectural forms. Second, because residential construction in China is restricted by the same strict planning regulations, the selected neighborhoods were also representative neighborhood patterns in other high-density cities in China. The floor area ratio distribution of the 100-sample data is shown in Figure 2, with 40% of the residential neighborhoods having floor area ratios in the range of 2.0–3.0 and the largest number of neighborhoods having floor area ratios around 2.5.

The building form induction analysis was carried out based on the summary of a sample of actual residential neighborhood cases in Wuhan, and several basic urban planning parameters were controlled within the same range in all cases in order to establish a common basis for performance comparison under the same planning conditions. In this study, 2.5 was used as the representative floor area ratio to generate the residential block types, and the simplified model plot size was set to 200 m × 250 m, i.e., 50,000 m². The high-rise tower residential buildings were set as 27 storeys, and mid-rise towers were set as 18 storeys. The high-rise slab residential buildings were set as 20 storeys, mid-rise slab residential buildings were set as 16 storeys, small high-rise slab residential buildings were set as 10 storeys, multi-story slab residential buildings were set as 6 storeys, and villas and low-rise slab residential buildings were both set as 3 storeys. For residential neighborhoods with mixed forms, the ratio of each neighborhood form type in the total building area was set equally at 1:1:1. Residential neighborhoods in this volume ratio were created and

divided into four representative urban neighborhood types (Figure 3): (1) single basic form (Simple), where the basic type was dominated by tower and slab types with different variations in height; (2) mixed form (Mixup), a two-by-two arrangement of tower and slab basic forms of different heights; (3) multiple forms (Multiple), a descending arrangement and combination of three basic forms of tower and slab of different heights by floor height; and (4) central integrated form (Center), consisting of low-rise linear buildings around the site and high-rise tower or slab buildings in the center of the site.

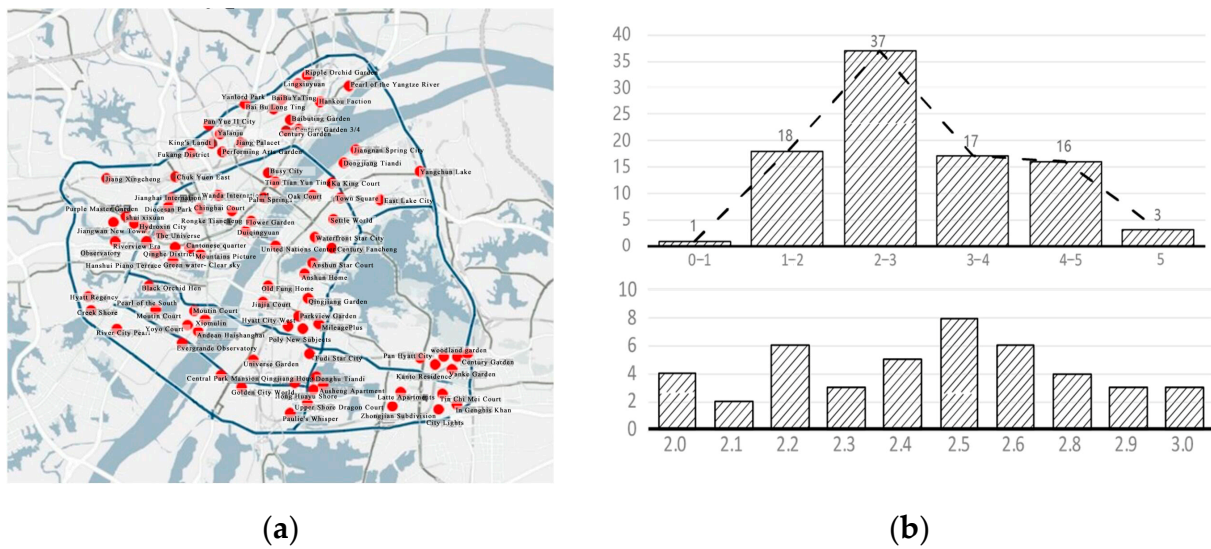


Figure 2. (a) Spatial Location Map of 100 Residential Block Samples in Wuhan; (b) Volume Ratio Distribution Map of 100 Residential Blocks and Distribution Map of Samples with Volume Ratios of 2–3.

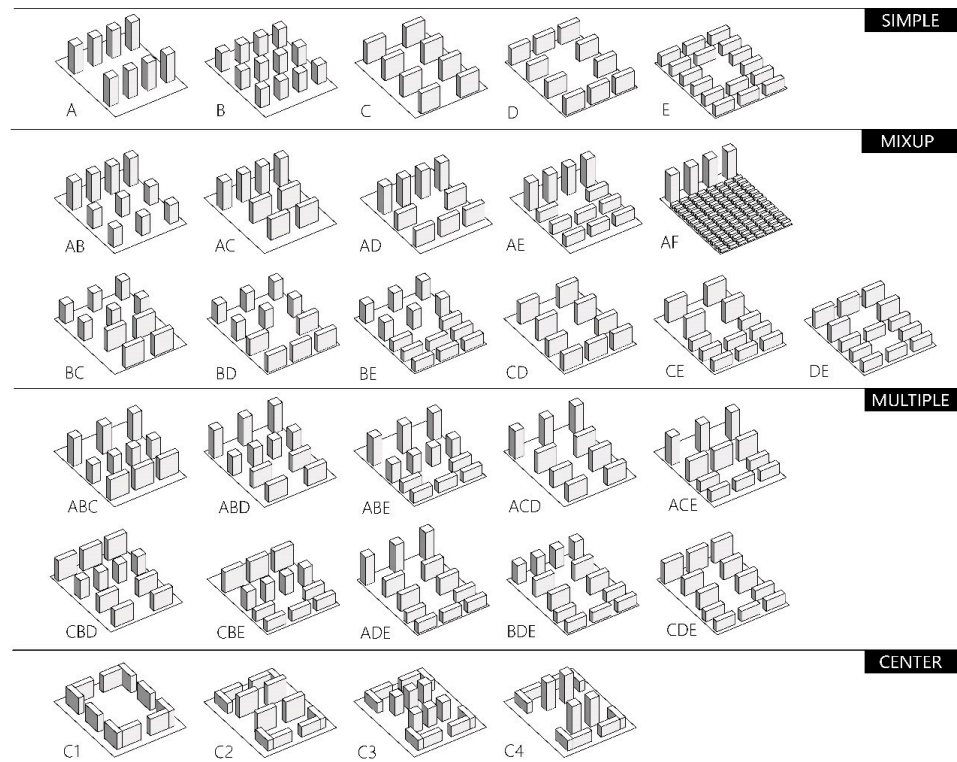


Figure 3. Thirty Typical Urban Residential Blocks of Four Types.

To theoretically test the performance of a given urban form in a homogeneous urban environment, the actual urban situation was simulated in an upper and lower block environment consisting of a 3×3 array of the same urban block type (Figure 4). Thus, in this scenario, the influence of the city block at the center of the array on its neighboring blocks, which was highlighted in Figure 4 in yellow, was “mirrored” back to the site and reflected in its own overall representation. The plot spacing was set to 30 m, representing the width of a typical neighborhood road. The left and right setback distances between the buildings and the site boundary were set to 5 m.

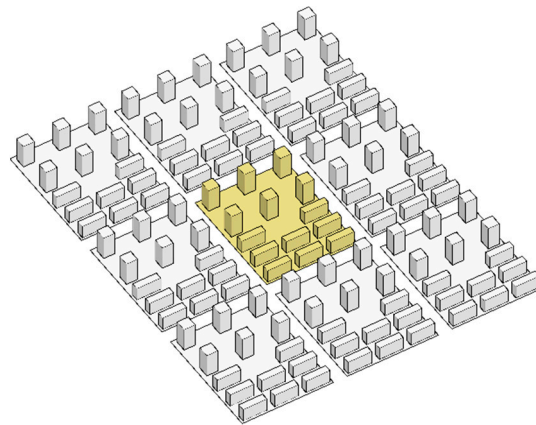
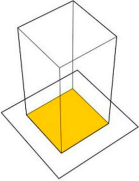
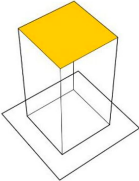
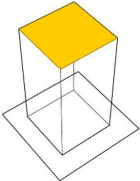
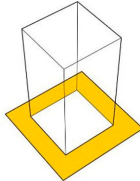
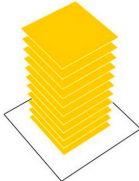
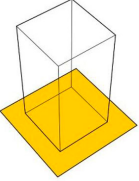
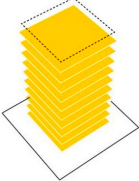
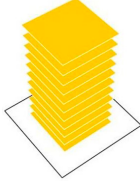
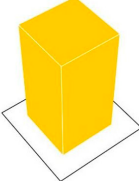
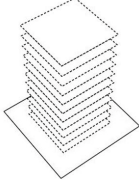


Figure 4. Simulated Environment of Residential Block.

3.2. Planning and Morphological Parameters Statistics

In order to describe the basic morphological characteristics of the above 30 settlement prototypes and obtain the correlations between the case morphological indicators and the final solar energy utilization, the relevant morphological parameters were extracted and the indicators were described, as shown in Table 1. The extracted parameters comprised two main levels.

Table 1. Building Planning and Geometric Parameters (the upper and lower diagrams represent the nominator and denominator in the calculation of a given parameter, respectively).

Building Site Coverage	Roof-to-Floor Area Ratio	Roof-to-Envelope Area Ratio	Open Space Ratio	Compacity	Area-to-Perimeter Ratio
					
Building Footprint Area	Roof Area	Roof Area	Open Space	Envelope Surface Area	Floor Surface Area
					
Site Area	Gross Floor Area (GFA)	Envelope Surface Area	Gross Floor Area (GFA)	Building Volume	Floor Surface Perimeter Length

The first-level indicators were designed to describe the basic morphology of the neighborhood, including the building density indicator of the neighborhood, which was

the ratio of the building footprint to the site area; the site open space ratio, which was the ratio of the open space area inside the site to the base area; and the ratio of the floor area to the perimeter of the floor. In addition, the average ratios of the area and volume of the maintenance structures of all buildings in the neighborhood were also calculated. The above indicators were intended to reflect the basic parameters of the case characteristics of each settlement.

The second-level indicators were used to describe the share of the roof in the radiant optimum receiving surface in the overall environment, including the roof area-to-floor area ratio and roof area-to-building maintenance structure area ratio. The roof area ratios in the settlement environment could affect the power generation yield of the PV system to a large extent.

According to the above description, the results of the extraction of morphological parameters for the different types of neighborhoods are shown in Table 2.

Table 2. Planning and Geometric Parameters of the Shape of 30 Typical Residential Buildings.

Typology	Case	GFA (m ²)	Site Coverage	Roof Area (m ²)	Envelope Area	Building Volume	Open Space Ratio	Avg Area-to-Perimeter Ratio	Compacity	Roof-to-Floor Area Ratio	Roof-to-Envelope Area Ratio
Simple	A	124,416	9.2%	4608	66,816	373,248	0.12	3.00	0.18	0.04	0.07
	B	131,328	13.8%	6912	69,120	373,248	0.12	3.00	0.19	0.05	0.10
	C	124,800	12.5%	6240	70,560	374,400	0.12	2.91	0.19	0.05	0.09
	D	124,800	15.6%	7800	72,120	374,400	0.11	2.91	0.19	0.06	0.11
	E	124,800	25.0%	12,480	76,800	374,400	0.10	2.91	0.21	0.10	0.16
Mixup	AB	124,416	23.0%	11,520	135,936	435,456	0.09	3.00	0.31	0.09	0.08
	AC	124,608	10.8%	5424	68,688	373,824	0.12	2.95	0.18	0.04	0.08
	AD	124,608	12.4%	6204	69,468	373,824	0.12	2.94	0.19	0.05	0.09
	AE	124,608	17.1%	8544	73,952	386,304	0.11	2.93	0.19	0.07	0.12
	AF	103,808	49.4%	24,704	116,288	239,616	0.11	1.74	0.49	0.24	0.21
	BC	121,152	13.2%	6576	69,840	373,824	0.12	2.96	0.19	0.05	0.09
	BD	121,152	14.7%	7356	70,620	373,824	0.11	2.95	0.19	0.06	0.10
	BE	121,152	19.4%	9696	75,104	386,304	0.10	2.94	0.19	0.08	0.13
	CD	121,680	14.0%	7020	71,340	374,400	0.11	2.91	0.19	0.06	0.10
	CE	121,680	18.7%	9360	75,824	373,824	0.11	2.91	0.20	0.08	0.12
DE	124,800	13.8%	6912	69,120	386,880	0.11	3.00	0.18	0.06	0.10	
Multiple	ABC	134,928	12.7%	6372	74,556	404,784	0.11	2.97	0.18	0.05	0.09
	ABD	138,048	17.5%	8748	77,904	414,144	0.10	2.93	0.19	0.06	0.11
	ABE	135,576	14.4%	7188	80,346	406,728	0.11	2.93	0.20	0.05	0.09
	ACD	130,896	12.8%	6408	73,152	392,688	0.11	2.93	0.19	0.05	0.09
	ACE	143,376	14.4%	7188	80,346	430,128	0.10	2.93	0.19	0.05	0.09
Center	C1	124,800	15.6%	7800	72,120	374,400	0.11	2.91	0.19	0.06	0.11
	C2	122,016	17.1%	8544	73,952	186,624	0.22	2.93	0.40	0.07	0.12
	C3	121,152	19.4%	9696	75,104	186,624	0.22	2.94	0.40	0.08	0.13
	C4	124,800	18.7%	9360	75,824	187,200	0.22	2.91	0.41	0.08	0.12

3.3. Building Energy Assessment

In order to evaluate the impact of these planning and morphological parameters on building energy use and their variation among urban neighborhood types, UMI (Urban Modeling Interface 3.0), a type of software developed by MIT's Sustainable Design Lab to quantify the full-cycle energy consumption and carbon emissions of buildings, was used in dynamic energy simulation to evaluate the output modeling of energy consumption in 30 residential neighborhood forms.

To eliminate the influence of factors other than those related to the building form, several settings in the energy modeling were controlled to be the same in all cases. Each building block type was divided vertically into storeys 3 m in height, and each storey was further subdivided into perimeter and core areas 3 m in depth to reflect the spatial and thermal correlations more realistically between the perimeter and interior spaces of the entire floor. According to the relevant standards [33], the north–south window-to-wall ratio for all exterior wall surfaces was specified as 0.4 and the east–west window-to-wall ratio was 0.35 in order to consider the impact of actual solar heat gain across the exterior glazed surfaces on energy consumption. No exterior or interior shading devices were modeled

since the focus of this study was on the overall geometric characteristics of the building form rather than the architectural design details.

Through on-site data research on the relevant residential neighborhoods in Wuhan and a review of relevant national codes and literature, the climate conditions, building envelope construction, system lighting, equipment operation time, and personnel activities in the hot summer and cold winter region were set in this study. Table 3 shows the general settings of the main parameters for typical residential buildings, which were applicable to each case of building energy modeling in UMI.

Table 3. Parameters and Settings for the Building Energy Simulation in UMI.

Parameter		Setting
Building Type		High-Rise Residential
Building construction	Roof	150 mm roll waterproof roof
	Floor surface	100 mm lightweight concrete
	Wall surface	200 mm concrete hollow block brick wall
	Window surface	3 mm clear glass double glazing with air gap Solar transmittance = 0.837
	Window-to-wall ratio	0.40 (South&North); 0.35 (East&West)
Internal loads	Equipment	5.0 W/m ²
	Lighting	7.0 W/m ²
	Cooling set point	26 °C
	Heating set point	18 °C
	Occupancy	0.03 population/m ²

3.4. Solar Power Assessment

In this study, two aspects were defined for the quantitative assessment of solar power generation level indicators for each neighborhood case, i.e., the total solar power generation under natural conditions and under conditions that satisfied certain radiation criteria. The quantification process started with obtaining the radiation distribution data on the building surfaces of each neighborhood using the solar radiation simulation tool. Then, the radiation data satisfying the conditions were processed using the module area method in the PV system power generation calculation formula, and the total power generation and the solar power generation of the neighborhood satisfying the threshold case were finally obtained.

First, for carrying out the radiation simulation of the case block, the study used the radiance calculation in the Honeybee module of the Ladybug Tools plug-in for Grasshopper in Rhino 7 software, obtaining the annual cumulative radiation of the unit building surface area. The meteorological conditions used in the simulation comprised the typical meteorological yearly data of Wuhan, which were obtained from a urban standard meteorological database with complete open source and high reliability.

Based on the radiation data obtained from the software simulation for different case blocks, the radiation data were converted into PV system power generation using Formula (1). The index was a comprehensive consideration of the level of radiation naturally received by each block case and the conversion efficiency problem of the PV system. The conversion formula conformed to the provisions specified in the national specification "Design Code for Photovoltaic Power Station" (GB50797-2012) for the calculation model of PV system power generation, and the calculation of PV system power generation was obtained as follows:

$$E_p = H_A \times A_{pv} \times \eta_i \times K \times (1 - R_d)^{N-1} \quad (1)$$

where H_A is the total annual cumulative solar irradiation on the building surface (kWh/m²*y); A_{pv} is the installable area of the PV module; N is the life cycle of the PV system; and η_i , K , and R_d are the photoelectric conversion efficiency, the integrated efficiency factor, and the decay rate of the PV system, respectively, which are taken as 19.1%, 86% [34], and 1.4%, respectively.

As previously mentioned, the power generation index needed to be quantified using two indicators. The total power generation under natural radiation conditions was calculated based on all radiation data for power generation. The total power generation under threshold conditions was calculated from the radiation data that met the threshold criteria. The threshold value, as the threshold of radiation intensity based on the economic balance considered during the whole life cycle of the PV system, is an important indicator controlling PV installation on building surfaces. This component should be quantified using the PV calculation formula and the PV system generation formula. The threshold calculation was performed combining the influence of various factors, such as subsidy policy, local electricity price, PV equipment installation cost, and service life. According to the input and output balance in Equation (2) over the whole life cycle of the PV system, calculation of the solar radiation threshold was obtained using Formula (3), as follows:

$$C_{sys} = t \times \eta_i \times K \times C_{ele} \times \sum_1^N (1 - R_d)^{N-1} \quad (2)$$

$$t = \frac{C_{sys}}{\eta_i \times K \times C_{ele} \times \sum_1^N (1 - R_d)^{N-1}} \quad (3)$$

where C_{ele} is the feed-in tariff, which is closely related to the national and local government's PV subsidy policy and taken as 0.9861 CNY/kWh in this study [35]. C_{sys} stands for the installed cost of the PV system, which mainly includes the initial investment in the system and the maintenance and operation costs, calculated as per Equation (4):

$$C_{sys} = C_{su} \times P_D \times (1 + R_{Ann} \times N) \quad (4)$$

where C_{su} indicates the installed cost of PV modules. According to the data published by the National Government Procurement Network [36] in early 2019, it is known that the installed cost of distributed PV systems ranges from 3.5 to 6.5 CNY/W. In this study, the system installation cost was set to 4 CNY/W. R_{Ann} is the annual system maintenance factor. P_D denotes the power density of PV modules. The power density of polycrystalline PV modules was set to 270 W/m² based on the results of our research on polycrystalline PV module products of relevant domestic PV companies. The values and settings of the relevant parameters are shown in Table 4.

Table 4. Parameter Settings and Data Sources for Solar Threshold Calculation.

Calculation Parameters		
Parameters		Settings and Sources
Installation Parameters	Total radiation (H_A)	Ladybug & Honeybee Simulation Tools
	Photovoltaic equipment installation area (A_{pv})	Threshold Criteria
Cost Parameter	PV feed-in tariff (C_{ele})	0.9861 CNY/kWh
	Integrated cost of photovoltaic system (C_{sys})	PV System Comprehensive Cost Formula
	Installation cost of photovoltaic system (C_{su})	4 CNY/W
Technical Parameters	Maintenance cost (A_{mm})	2%
	Photovoltaic system power density (P_D)	270 W/m ²
	Photovoltaic system life cycle (N)	0~25 Years
	Conversion efficiency of photovoltaic system (η_{pv})	16%
	Comprehensive efficiency of photovoltaic system (K)	86%
	PV system attenuation rate (R_d)	1.40%

In this study, polycrystalline silicon PV modules were adopted, and the relevant coefficients were obtained by determining the performance of the same type of product in the industry in combination with national policies and other indicators to obtain the corresponding data. The parameter settings and data sources are listed in the following table:

Thus, based on the above establishment of the solar radiation threshold formula, the solar radiation thresholds of PV systems under different life cycles (0–25 years) were calculated to analyze the solar radiation thresholds in relation to the system life cycle. The results showed that the solar radiation threshold gradually decreased with increasing system life cycle duration. In this study, a system life cycle of 20 years was chosen as the standard, a solar radiation threshold value of $530 \text{ kWh/m}^2\cdot\text{y}$ was determined in Wuhan, and the corresponding system installation cost was 1512 CNY/m^2 .

3.5. Comprehensive Energy Efficiency Assessment and Integration Workflow

In order to comprehensively assess energy use efficiency and solar photovoltaic (PV) module power generation efficiency, the study partially superimposed energy consumption and energy output to quantify the combined energy-saving and carbon-reducing efficiencies of the neighborhood form and also to determine which residential neighborhood type had the highest comprehensive energy efficiency. Self-sufficiency coefficients based on energy consumption and use were compared for different neighborhoods. To facilitate the simulation and performance evaluation of solar potential, energy intensity, and comprehensive energy efficiency levels, the Urban Modeling Interface (UMI) platform and Rhino software's Grasshopper parametric modeling with its Ladybug plug-in and Honeybee component were employed in this study to create an integrated workflow for building energy consumption and solar radiation simulation calculations. Weather data in EPW file format for Wuhan, China, were used as the input for the solar radiation and building energy consumption simulations, including statistically representative data for certain key meteorological parameters, such as hourly horizontal radiation, wind speed, dry bulb temperature, and relative humidity.

As for the workflow, Google satellite maps were used to capture neighborhood contours and patterns, and then a 3D neighborhood model of the city was built in Rhino using research measurements, integrated with the Ladybug plug-in and Honeybee tool on the Grasshopper parameterization platform. The Grasshopper platform and radiance computational engine were invoked to perform solar radiation simulations on the 3D model in Rhino [37]. This radiation simulation method was able to integrate building size, orientation, and relevant details, such as ground and adjacent building reflections, to obtain realistic radiation values for the block roof and each façade in the case model. In the energy consumption simulation, the UMI platform was adopted to input regional climate conditions, building envelope construction parameters, system lighting, equipment operating hours, and personnel activities through research and code review to simulate the energy consumption of the completed 3D model and derive the total energy consumption load of the neighborhood building. The above processes are shown in Figure 5.

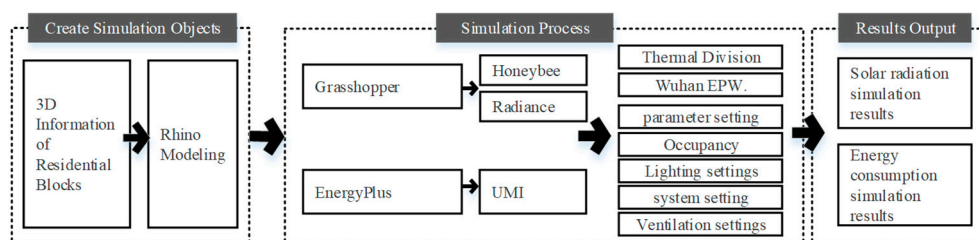


Figure 5. Integrated Simulation Workflow.

4. Results

4.1. Analysis of Energy Consumption Simulation Results

Based on the simulation calculation method of building energy intensity in residential neighborhoods mentioned above, the results of the annual operational energy intensity measurements per unit of building area for different types of residential neighborhoods were obtained, in which the total energy intensity included cooling energy intensity per unit of building area, heating energy intensity per unit of building area, lighting energy intensity per unit of building area, and equipment energy intensity per unit of building area. As can be seen from the energy intensity data per unit of floor area in each block, some variations were observed in the building energy intensity across the case blocks (Table 5); the overall total average energy intensity value of each block varied between 58 and 63 kWh/m²*y, with no wide range of fluctuations. The energy intensity results are shown in Figure 5.

Table 5. Building Energy intensity Data.

Typology	Case	Total Building Energy Consumption (kWh/m ²)	Heating Energy Consumption (kWh/m ²)	Cooling Energy Consumption (kWh/m ²)
Simple	A	58	5	10
	B	60	5	11
	C	60	6	12
	D	59	5	9
	E	61	6	11
Mixup	AB	59	5	12
	AC	59	4	10
	AD	59	5	10
	AE	59	5	10
	AF	63	8	11
	BC	59	5	12
	BD	59	5	11
	BE	60	6	11
	CD	59	5	10
	CE	59	6	11
DE	60	5	11	
Multiple	ABC	59	5	10
	ABD	59	5	11
	ABE	59	5	10
	ACD	59	5	11
	ACE	59	5	10
	CBD	59	5	10
	CBE	59	5	10
	ADE	59	5	11
	BDE	59	5	10
CDE	59	5	12	
Center	C1	59	5	11
	C2	60	6	11
	C3	60	6	11
	C4	60	6	10

The total energy load and annual cooling and heating energy intensity data for a typical morphological block are shown in Figure 6. According to the results, the total energy intensity of the building fell in the range of 58–63 kWh/m²*y, with the maximum value being 1.09 times the minimum value, indicating that the block form parameters had a great impact on the building energy intensity under the same building volume ratio and land area. The analysis results indicated that in terms of heating energy intensity, case AF

(high-rise tower–multi-story slab) had the highest block energy intensity of 8 kWh/m²*y, being twice that of the lowest case, case AC (4 kWh/m²*y), and the average distribution of heating energy intensity in most cases was 5 kWh/m²*y. Cases C, AB, BC, and CDE (12 kWh/m²*y) had the highest cooling energy intensity, with case CDE (12 kWh/m²*y) being 1.34 times that of case D (9 kWh/m²*y), and the cooling energy intensity of most cases was distributed between 10 and 11 kWh/m²*y on average. The analysis results from the total energy intensity of each type showed that case AF (high-rise tower–multi-story slab) reached the highest total energy intensity per unit floor area at 63 kWh/m²*y, which was 1.09 times greater than that of the lowest energy intensity case, case A (high-rise tower, 58 kWh/m²*y), and the average total energy intensity of most of the remaining case forms remained around 59 kWh/m²*y. Comparing the analysis results of the four types (single basic form, mixed form, multiple form, and central integrated form), the multiple form block type (Multiple) was more stable with greater energy-saving potential.

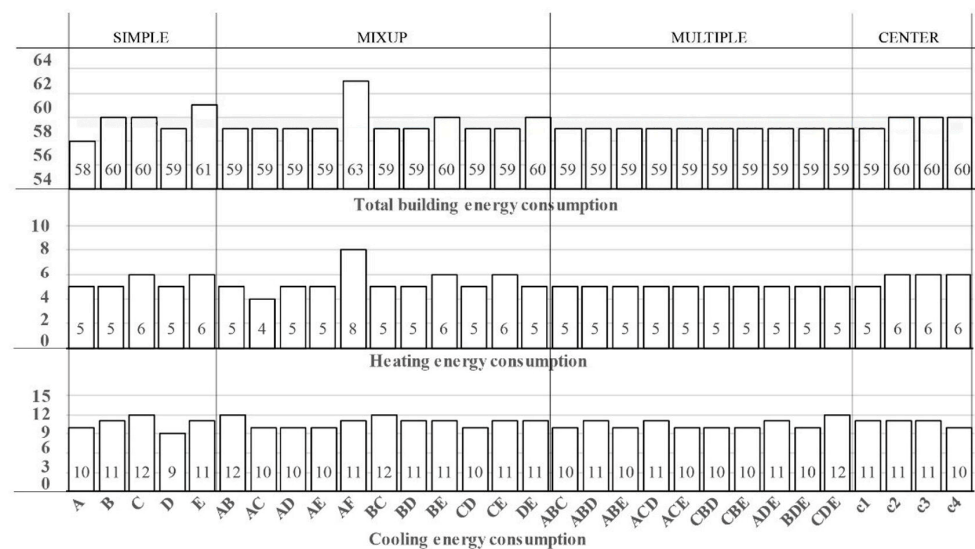


Figure 6. Results Related to Building Energy Consumption for the 30 Cases Grouped by Typology.

4.2. Solar Power Simulation

Likewise, some variations were found in the solar energy reception potential across the case neighborhoods, as manifested in the graph of the average natural radiation received by each neighborhood. The overall average radiation of each neighborhood varied between 460 and 500 kWh/m²*y without a wide range of fluctuations. The BE neighborhood reached the highest average natural radiation reception at 498.33 kWh/m²*y. The ABC, AC, and C2 neighborhoods had the lowest average radiation reception of between 460 and 461 kWh/m²*y. The average radiation received in each neighborhood was below the threshold standard (Figure 7).

The above describes the average level of natural radiation reception in each neighborhood. Considering the large variation in natural radiation, the magnitude of the average radiation in each neighborhood that met the threshold needed to be considered to assess the actual solar power potential of each neighborhood. As shown in the graph of the average radiation of the portion of each neighborhood that met the threshold, a large difference could be discovered in the trend of the average radiation of each neighborhood that met the threshold and the average natural radiation. As shown in the graph, the overall average radiation ranged from 960 to 1060 kWh/m²*y. Block E had the highest average radiation of 1063.5 kWh/m²*y. Block C2 reached the lowest radiation, with an average radiation value of 960.3 kWh/m²*y. From this graph, it could be observed that the average radiation value of the part meeting the threshold was much larger than the threshold standard, reflecting the nonlinear distribution of the overall radiation.

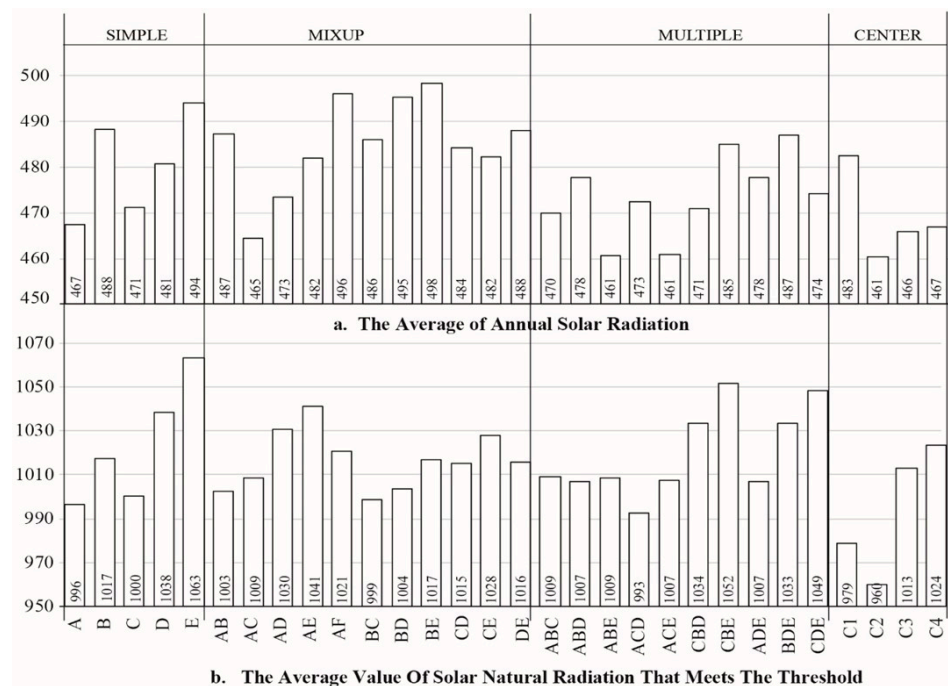


Figure 7. (a) Average Annual Solar Radiation; (b) Average Value of Solar Natural Radiation that Met the Threshold.

Considering the non-uniformity of radiation distribution, the percentage of radiation in different ranges in each block was counted. As shown in the figure below, the overall radiation exposure was mainly concentrated in the neighborhoods. On the whole, the dwelling radiation was mainly concentrated below $350 \text{ kWh/m}^2\cdot\text{y}$. The radiation was the least distributed within $650\text{--}1050 \text{ kWh/m}^2\cdot\text{y}$. The part with radiation greater than $1050 \text{ kWh/m}^2\cdot\text{y}$ accounted for the second largest proportion. It could be seen that the part with the average radiation value meeting the threshold mostly satisfied $>1050 \text{ kWh/m}^2\cdot\text{y}$, and the radiation in this part mainly came from the roof, which, therefore, made a great contribution to the PV power generation system.

4.3. Effect of Different Block Form Parameters on Energy Intensity

According to the results of the scatter plots and regression analysis of the 30 cases of planning geometric parameters and total energy intensity per unit of floor area in the neighborhood, as shown in Figure 8, site coverage, compacity, and the roof envelope area ratio were relatively the most significant influencing factors on the total energy intensity, with each influencing parameter having a variance of slightly more than 60%, followed by the roof-to-floor area ratio (59.7%), while other planning geometric parameters, such as the open space ratio and Avg APR, showed lower correlations with the total energy intensity of the neighborhood. This suggested that, in the design of urban residential neighborhoods under the same planning conditions, types with relatively higher site coverage, roof-to-floor areas, and GFA ratios might realize greater energy-saving potential under the same circumstances (considering building shading) (Figures 8 and 9).

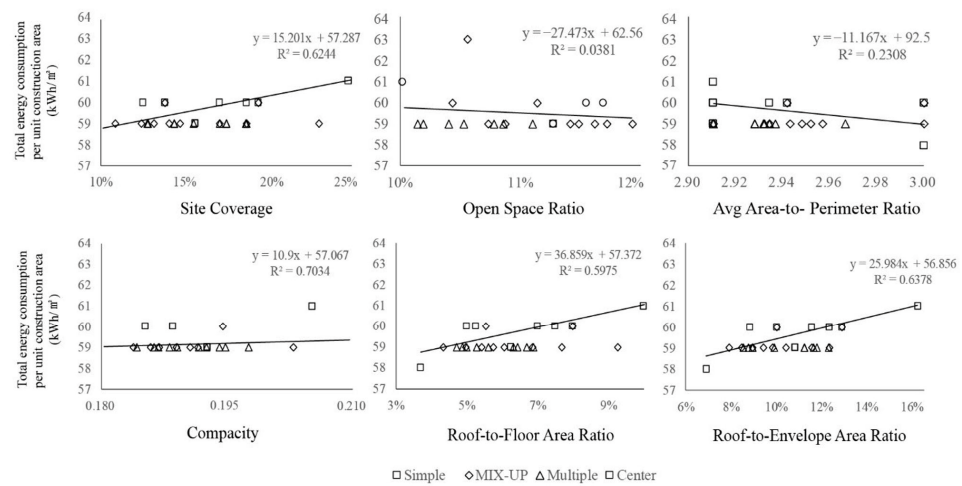


Figure 8. Results of Scatter Plots and Linear Regression Analysis of the Total Net Energy Use Intensity of Buildings and Planning and Geometric Parameters.

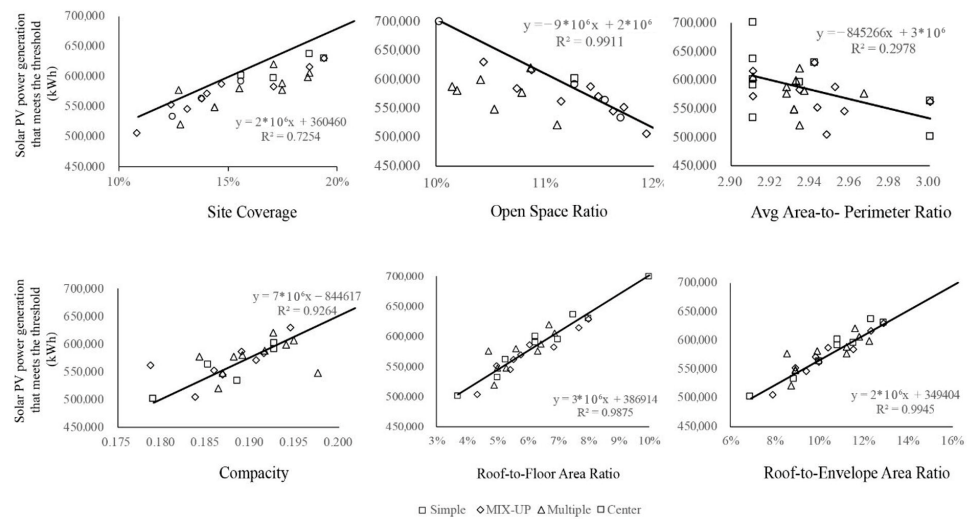


Figure 9. Scatter Plots of Solar Power Generation that Met the Threshold, Planning and Geometric Parameters, and Results of Linear Regression Analysis.

Regression analysis of the radiation data and the selected morphological parameters for each neighborhood meeting the threshold was performed, and the results are shown in the following figure. The results showed that four of the six indicators showed strong correlations with the solar radiation that met the threshold, and their degrees of correlation were more than 90%. Among them, the open space ratio, roof-to-floor area ratio, and roof-to-envelope area ratio were the indicators most correlated with the radiation data, with R^2 values of 0.9911, 0.9875, and 0.9945, respectively. The correlation coefficients between the other two indicators, building density and floor area-to-perimeter ratio, and the radiation data meeting the threshold were 72.54% and 29.78%, respectively. Meanwhile, except for the open space and floor area-to perimeter ratios presenting negative correlations with the radiation data, the remaining four indicators displayed positive correlations. From the above data analysis, it could be found that the correlation between the building roof, as an important receiving surface of solar radiation, and the radiation data that met the threshold value was the most significant.

4.4. Comprehensive Energy Efficiency Analysis

Considering that the block space type affected both the efficiency of energy use and solar PV module power generation, the energy consumption and energy output

components were superimposed in this study to quantify the comprehensive energy and carbon reduction efficiency of the block form. Figure 10 summarizes the analysis of solar PV power generation potential versus total energy use per unit building area of the neighborhood for 30 cases of residential neighborhood forms after comprehensive carbon reduction adjustment. From the figure, it can be seen that the neighborhood forms of AB (mixed high-rise slab and high-rise tower) and AF achieved the highest PV power generation capacity, followed by the power generation potential of type E, while case types AF, B, and C reached the lowest building energy intensity (Figure 10).

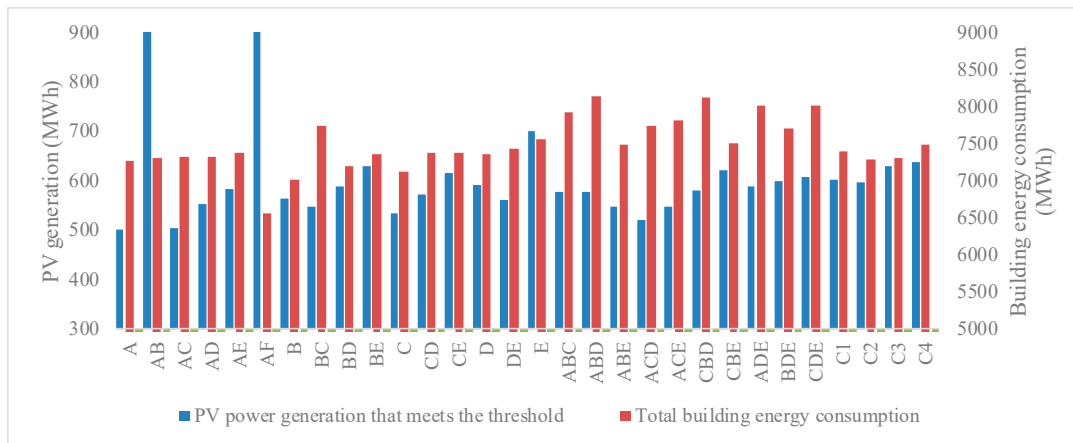


Figure 10. Comparison of Total Photovoltaic Power Generation that Met the Threshold and Energy Consumption of the Block.

In order to further determine which residential block type had the best energy efficiency, a comparison of the self-sufficiency factor was performed. The AF case type (high-rise tower + villa) had the best energy-saving potential, which was attributed to the advantage of less mutual shading between buildings and the largest building roof area ratio (49.4%), providing the strongest potential for installing solar PV panels. However, due to the policy guidance of highly intensive land use in China, this block type is not recommended for development in urban centers. This result was followed by the comprehensive energy-saving potential of the AB type, while the E and CBE types were in third and fourth places respectively, with a large gap fall (Figure 11).

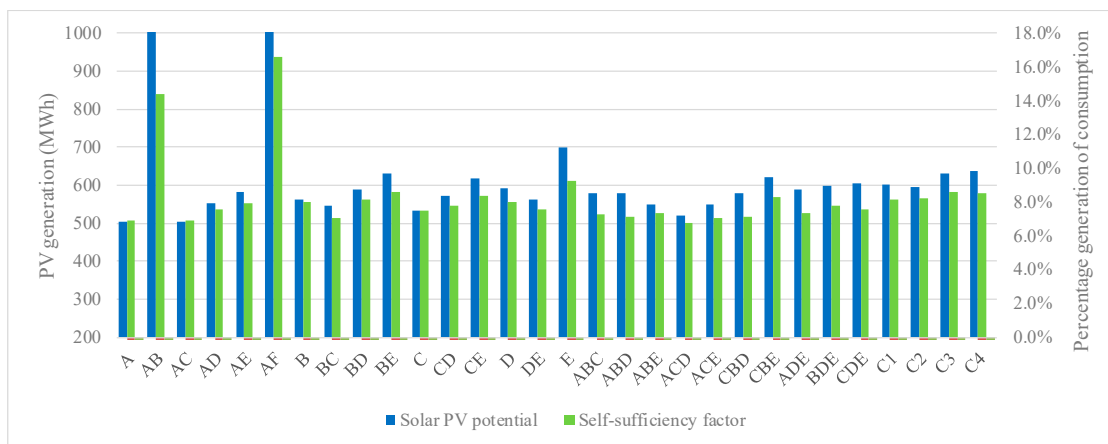


Figure 11. Comparison of Photovoltaic Power Generation Meeting the Threshold and Building Energy Consumption Self-sufficiency Ratios.

4.5. Development Strategy for Renewable Energy

Based on the energy efficiency analysis in Section 3.4, large differences were observed in the energy efficiency of different forms of settlements as well as in the contribution of power generation on the surfaces of different buildings in the same settlement. Therefore, it was necessary to analyze the development generation strategy for different blocks, as well as for the same block. The benefits of the location and method of solar energy development under natural radiation conditions and threshold control conditions were evaluated.

First of all, the solar radiation ranges for different types of neighborhoods were analyzed. From the box plots of the radiation results, it could be seen that the radiation distribution on each façade in each neighborhood case mostly showed regular characteristics, namely varying within a certain range. Among them, the roof was the most valuable building façade, and the solar radiation it could receive was the most stable and had the highest value, all distributed above 1000 kWh/m²*y. The solar radiation received by the north façade was also more stable, but it failed to meet the threshold value, fluctuating around 300 kWh/m²*y, with the lowest utilization value. The amount of solar radiation received by the south façade was significantly affected by the environment, and the radiation was mainly distributed within 500–600 kWh/m²*y, with fewer values available under the threshold limit. The radiation distribution of the east elevation was generally lower than that of the south elevation, floating on the line of 400 kWh/m²*y, and the utilization value was not high. Finally, the radiation of the west elevation was most influenced by the environment, and the radiation distribution was larger, mainly varying 400–600 kWh/m²*y, with the same usable value as the south elevation (Figure 12).

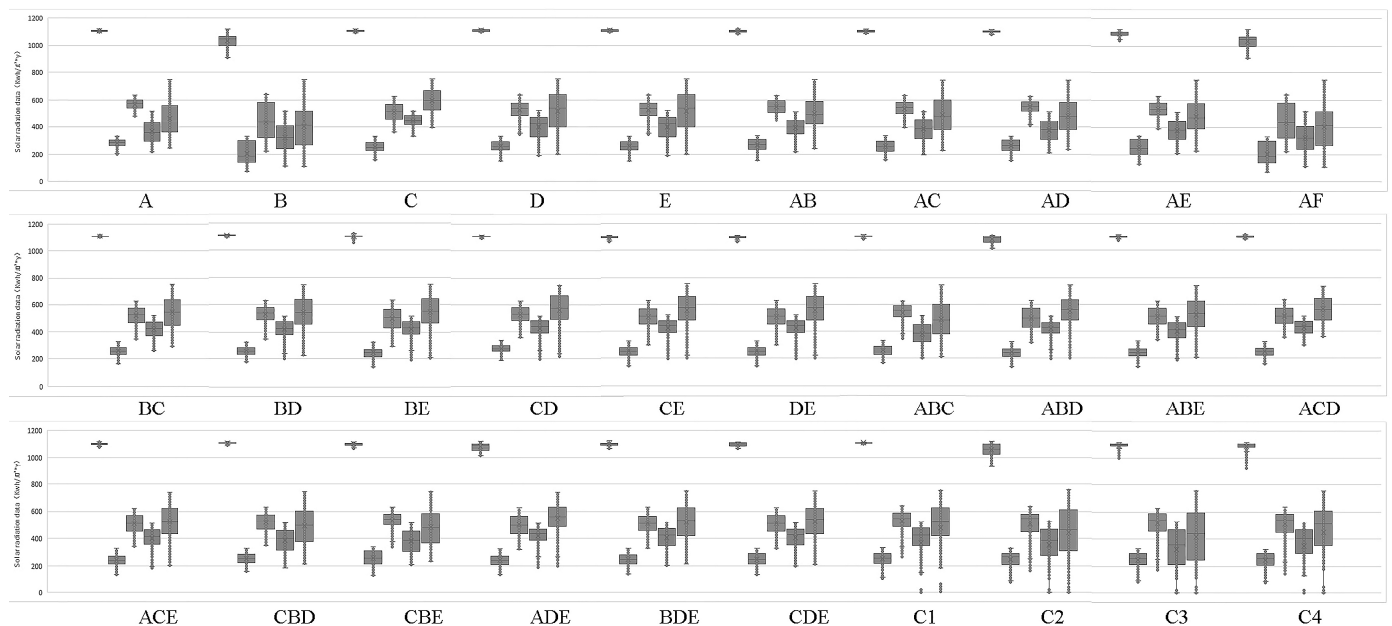


Figure 12. Distribution of Solar Radiation on Each Façade of 30 Residential Blocks.

The neighborhoods showed similar patterns in the percentage of the fraction meeting the threshold. The AF neighborhood had the highest percentage of greater-than-threshold data, at 24%. Block A, on the other hand, had the lowest threshold fraction at 9%. As a whole, the proportion of the radiation-receiving area that met the threshold was not high in the overall block, while the data with radiation levels below 530 kWh/m²*y accounted for the major part. It could be seen that the introduction of threshold criteria could have a large impact on the revenue of PV systems in the implementation of actual PV installation projects.

By conducting interval percentage statistics of solar radiation in each case block, the same trends of change could be found in the percentage of radiation between different types

of blocks (Figures 13 and 14). The percentage of the portion meeting the threshold value in each case was around 15%. When the threshold standard was changed between 700 and 1000 kWh/m²*y, the percentage meeting the threshold in each case neighborhood did not fluctuate greatly, and the percentage stabilized around 11%. When the threshold standard was lowered, it could be found that the threshold case curve in each case underwent a large change. From greater than 200 kWh/m²*y to greater than 600 kWh/m²*y, the proportion of radiation data meeting the condition dropped from about 95% to 18% (Table 6). From the above data, it could be found that the proportion of radiation data distributed from 200 to 700 kWh/m²*y was relatively large and varied evenly. In the part that met the threshold value, the radiation data were mostly concentrated between 1000 and 1100 kWh/m²*y (Table 7). Combined with the building envelope radiation distribution data, this part of the radiation was mostly derived from the roof of the building; thus, it could be found that the contribution of radiation reception from the roof of the building was higher under consideration of the threshold value.

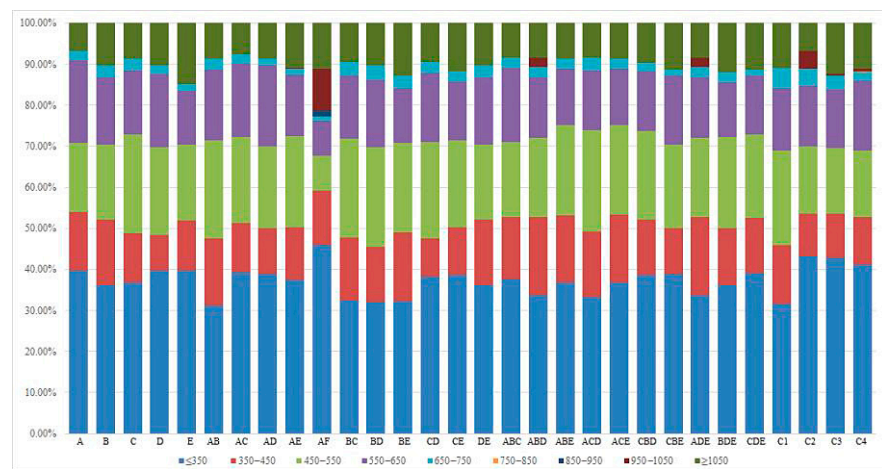


Figure 13. Solar Radiation Interval Ratio Chart of 30 Residential Blocks.

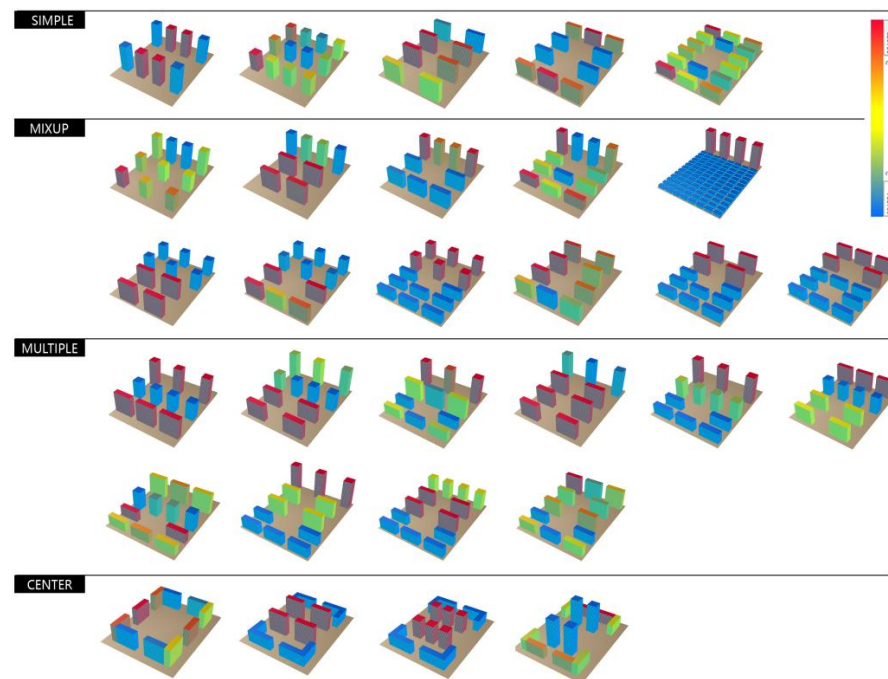


Figure 14. Visualization of Annual Cumulative Energy Intensity on Building Envelope Surfaces.

Table 6. Proportion of Solar Radiation that Met the Corresponding Standard.

Typology	Case	≥100	≥200	≥300	≥400	≥500	≥600	≥700	≥800	≥900	≥1000	≥1100	≥1200
Simple	A	100.00%	100.00%	76.20%	52.40%	40.20%	16.90%	7.80%	6.70%	6.70%	6.70%	6.00%	0.00%
	B	100.00%	99.10%	76.60%	56.60%	37.50%	19.90%	11.70%	10.30%	10.30%	10.30%	9.50%	0.00%
	C	100.00%	97.20%	68.70%	60.80%	38.50%	16.60%	10.00%	8.60%	8.60%	8.60%	7.70%	0.00%
	D	100.00%	97.30%	68.20%	57.20%	41.90%	18.50%	11.40%	10.30%	10.30%	10.30%	9.40%	0.00%
	E	100.00%	93.20%	67.60%	54.90%	39.10%	20.30%	15.60%	14.80%	14.80%	14.80%	14.30%	0.00%
	Average	100.00%	97.40%	71.50%	56.40%	39.40%	18.50%	11.30%	10.10%	10.10%	10.10%	9.40%	0.00%
Mixup	AB	100.00%	99.00%	80.40%	61.20%	38.90%	19.00%	9.20%	8.60%	8.60%	8.60%	6.10%	0.00%
	AC	100.00%	97.10%	72.40%	55.70%	38.20%	15.80%	8.50%	7.70%	7.70%	7.70%	5.50%	0.00%
	AD	100.00%	97.50%	73.90%	56.20%	41.10%	16.90%	9.30%	8.60%	8.60%	8.60%	4.90%	0.00%
	AE	100.00%	93.70%	75.50%	57.70%	40.00%	19.40%	11.60%	11.10%	11.10%	11.10%	3.10%	0.00%
	AF	100.00%	81.70%	67.40%	48.10%	35.80%	29.80%	23.10%	22.80%	22.80%	17.10%	1.80%	0.00%
	BC	100.00%	98.10%	74.80%	62.30%	38.10%	18.40%	10.80%	9.40%	9.40%	9.40%	9.20%	0.00%
	BD	100.00%	98.40%	73.90%	63.00%	41.30%	19.60%	12.00%	10.30%	10.30%	10.30%	9.20%	0.00%
	BE	100.00%	95.40%	73.20%	60.50%	38.80%	21.60%	14.10%	12.70%	12.70%	12.70%	8.10%	0.00%
	CD	100.00%	99.90%	72.20%	59.20%	40.80%	17.50%	10.70%	9.40%	9.40%	9.40%	8.20%	0.00%
	CE	100.00%	95.20%	69.20%	57.00%	38.80%	20.10%	12.90%	11.80%	11.80%	11.80%	5.00%	0.00%
	DE	100.00%	99.10%	76.70%	56.60%	37.50%	19.90%	11.70%	10.30%	10.30%	10.30%	9.40%	0.00%
	Average	100.00%	95.90%	73.60%	58.00%	39.50%	19.80%	12.20%	11.20%	11.20%	10.60%	6.40%	0.00%
Multiple	ABC	100.00%	97.80%	71.90%	55.60%	38.40%	17.30%	9.40%	8.50%	8.50%	8.50%	6.00%	0.00%
	ABD	100.00%	95.10%	72.30%	60.40%	35.80%	19.30%	11.60%	10.80%	10.80%	10.80%	3.70%	0.00%
	ABE	100.00%	95.00%	69.40%	58.10%	34.00%	16.20%	9.30%	8.60%	8.60%	8.60%	4.60%	0.00%
	ACD	100.00%	96.70%	72.20%	62.50%	36.40%	16.90%	9.40%	8.40%	8.40%	8.40%	5.00%	0.00%
	ACE	100.00%	94.90%	69.40%	58.20%	33.90%	16.00%	9.30%	8.60%	8.60%	8.60%	5.30%	0.00%
	CBD	100.00%	97.30%	69.40%	56.30%	36.00%	17.10%	10.50%	9.70%	9.70%	9.70%	8.50%	0.00%
	CBE	100.00%	94.80%	74.50%	56.40%	40.60%	18.40%	11.90%	11.40%	11.40%	11.40%	6.10%	0.00%
	ADE	100.00%	95.00%	72.30%	60.40%	35.80%	19.20%	11.60%	10.80%	10.80%	10.80%	3.40%	0.00%
	BDE	100.00%	95.80%	70.90%	59.40%	37.40%	19.40%	13.00%	12.00%	12.00%	12.00%	7.40%	0.00%
	CDE	100.00%	94.30%	69.10%	56.40%	36.00%	18.20%	11.90%	11.30%	11.30%	11.30%	6.40%	0.00%
Average	100.00%	95.70%	71.10%	58.40%	36.40%	17.80%	10.80%	10.00%	10.00%	10.00%	5.70%	0.00%	
Center	C1	92.00%	89.50%	74.50%	63.10%	41.40%	22.10%	13.20%	10.90%	10.90%	10.90%	10.90%	0.00%
	C2	95.00%	89.80%	67.10%	51.70%	39.40%	20.40%	13.30%	11.10%	11.10%	9.90%	2.70%	0.00%
	C3	95.00%	86.40%	66.30%	52.70%	37.60%	21.50%	14.30%	12.70%	12.70%	12.70%	6.30%	0.00%
	C4	95.00%	89.20%	68.60%	54.10%	38.10%	19.80%	12.70%	11.80%	11.80%	11.60%	4.10%	0.00%
	Average	94.00%	88.70%	69.10%	55.40%	39.10%	21.00%	13.40%	11.60%	11.60%	11.30%	6.00%	0.00%

Table 7. Average Solar Radiation.

Typology	Case	Average of Annual Solar Radiation (kWh/m ² *y)	Average Value of Solar Radiation That Meets Threshold (kWh/m ² *y)
Simple	A	467.38	996.28
	B	488.28	1017.36
	C	471.27	1000.50
	D	480.78	1038.35
	E	494.11	1063.48
Mixup	AB	487.35	1002.58
	AC	464.51	1008.67
	AD	473.35	1030.45
	AE	482.04	1041.33
	AF	496.20	1020.74
	BC	485.97	998.55
	BD	495.42	1003.79
	BE	498.34	1017.13
	CD	484.28	1015.35
	CE	482.31	1027.76
DE	488.02	1015.65	

Table 7. Cont.

Typology	Case	Average of Annual Solar Radiation (kWh/m ² *y)	Average Value of Solar Radiation That Meets Threshold (kWh/m ² *y)
Multiple	ABC	469.86	1009.02
	ABD	477.76	1007.18
	ABE	460.75	1008.74
	ACD	472.56	992.70
	ACE	460.84	1007.35
	CBD	470.91	1033.62
	CBE	484.92	1051.72
	ADE	477.74	1006.69
	BDE	487.12	1033.22
	CDE	474.10	1048.60
Center	C1	482.57	978.77
	C2	460.51	960.28
	C3	466.03	1012.86
	C4	466.92	1023.72

The average radiation values considering the threshold case were compared and analyzed. From Table 8, it could be found that both combined block cases exhibited the highest average radiation in both natural radiation acceptance and threshold-meeting radiation reception, with 188.00 and 55.00 kWh/m²*y per unit of land area, respectively. For the natural radiation-receiving amount, the enclosed type had the lowest average radiation amount, with 164.05 kWh/m²*y per unit land area. In the comparison of radiation averages that satisfied the threshold, the single form neighborhood case reached the lowest average radiation with only 44.74 kWh/m²*y per unit of land area. In the graph of natural radiation reception, it could be seen that the data for single form cases, three types of styles, and the enclosed style were more stable. The difference between the data for two types of cases was large, in which the radiation per unit land area of the AB type neighborhood reached 316.58 kWh/m²*y, which was the highest radiation intensity among all cases. In second place was the AF case, with a radiation value of 267.23 kWh/m²*y. In the threshold control case, the AF block had the highest radiation performance with 130.37 kWh/m²*y per unit land area, which was the highest among all block cases.

Table 8. Solar Data per Unit Area.

Typology	Case	Solar Radiation per Unit Area (kWh/m ² *y)	The Amount of Solar Radiation That Meets the Threshold Unit Area (kWh/m ² *y)
Simple	A	147.47	28.75
	B	163.13	45.01
	C	160.23	39.32
	D	163.18	43.90
	E	187.37	66.72
Mixup	AB	316.58	73.55
	AC	152.25	32.92
	AD	155.00	34.89
	AE	167.44	45.55
	AF	267.23	130.37
	BC	163.79	43.22

Table 8. Cont.

Typology	Case	Solar Radiation per Unit Area (kWh/m ² *y)	The Amount of Solar Radiation That Meets the Threshold Unit Area (kWh/m ² *y)
Mixup	BD	166.83	46.88
	BE	177.73	57.98
	CD	164.51	41.79
	CE	173.44	52.89
	DE	163.04	44.91
Multiple	ABC	167.82	39.76
	ABD	174.95	48.91
	ABE	175.81	42.51
	ACD	164.28	39.55
	ACE	175.85	42.67
	CBD	176.41	45.69
	CBE	170.19	47.54
	ADE	174.94	48.93
	BDE	174.98	53.27
CDE	177.96	50.58	
Center	C1	161.86	52.19
	C2	160.09	51.13
	C3	166.20	58.06
	C4	168.04	52.11

5. Discussion

On the basis of a typological approach, the influence of urban settlement form on the overall energy efficiency of buildings was investigated, and the correlations between the main neighborhood form indicators and the energy consumption and solar power generation of settlement buildings were respectively quantified, providing a reference for the layout planning and building form design of new urban settlements for energy-saving purposes. In reality, however, the influencing factors and relationships are often more complex, and the shortcomings of this study are discussed below.

Based on the morphological classification method, four major categories and 30 sub-categories of settlement prototypes were extracted from Chinese urban settlements, and the energy-saving effects of each morphological settlement were explored. Since the focus of this study was mainly on Chinese cities, the findings lack applicability to urban settlements in other regions outside of China. However, urban settlements in China have certain regular characteristics in terms of morphological layout, height, and spacing under national and local building design codes, so the findings of this study still have wide-ranging applications.

In this study, when analyzing the energy consumption problem, the influence of human activities in the energy consumption model was simplified in order to quickly obtain energy consumption data for a larger number of neighborhoods. Although human activities [38] have an impact on building energy consumption, it is not the main subject of discussion in this study, which was mainly focused on the energy efficiency of buildings under the influence of settlement form. To more comprehensively quantify the energy consumption of settlements, the human activities in different types of settlements will be further explored through field studies in the future.

There are also limitations in the simulation of energy consumption in neighborhood buildings and in the assessment of solar power potential. First, the outdoor environment, the way the building is constructed, and indoor human behavior patterns all have impacts on the energy consumption of the building in a neighborhood simulation study. Since the influence of urban form elements was mainly explored in this study, the above variables were set to constant values in order to maintain the control variables in the simulation study.

Secondly, solar power potential was studied in the process of building prototype construction, and the discount factors were set to express the impact of building surface concavity and equipment on PV installation, as well as the attenuation of power generation by PV panels themselves due to the outdoor environment, both by research and drawing on empirical values from other related literature. In subsequent research, the influence of outdoor temperature on PV power generation and shading from building surface concavity on its radiation can be discussed and analyzed in depth.

6. Conclusions

6.1. Urban Settlement Form Affects Comprehensive Energy Consumption and Solar Energy Development, and the Assessment of the Energy Efficiency of Settlements Should Focus on the Trade-Offs between Planning and Design Parameters, with a Mix of High and Low Configurations Preferred for the Selection of Neighborhoods

The above data and analysis reveal that the settlement form has an impact on both energy consumption and renewable energy development in buildings within settlements. By quantifying both aspects in different settlement forms, the correlations between settlement form indicators and the two aspects, as well as the overall energy efficiency of different settlement forms, were assessed.

The neighborhood morphological indicators selected for the study maintained high degrees of correlation with both neighborhood energy intensity and solar power potential, and the quantification of these indicators and regular correlations can better guide urban settlement layout planning. The results of the analysis of the total energy intensity per unit of floor area showed that site coverage, floor area ratio, and roof enclosure area ratio were relatively the most significant influencing factors, followed by the roof-to-ground area ratio. In the design of an urban residential subdivision under the same planning conditions, the type with a relatively higher site coverage, roof footprint, and total floor area ratio may realize greater potential for energy savings, with four of the six indicators showing strong correlations with the amount of solar radiation that reached the threshold, with correlations of 90% or more.

The correlations between the double quantification results and the neighborhood form can also be interpreted for the individual neighborhood case, where the AF form was a mixed form with low-rise housing and high-rise towers. The energy intensity of this form of settlement was the highest among the 30 neighborhood cases. In terms of solar power performance, however, the AF block type had much higher solar power capacity than the other block types. This was mainly because the smaller residential spacing of low-rise houses increases the roof area in the neighborhood to receive solar radiation, which leads to an increase in radiant power generation for the same building volume index. Therefore, the AF block showed the best energy efficiency in the comprehensive energy efficiency assessment.

As can be seen from the above cases, it is not possible to quantify the energy-saving effect of a neighborhood in a comprehensive manner only from the perspective of a single energy consumption or renewable energy development indicator. Among the 30 forms of urban settlements compared in this study, the settlements with the lowest energy consumption levels were not in a dominant position in terms of solar energy resource development, and thus led to low levels of comprehensive energy savings. Although low-rise residential settlements with good energy efficiency, represented by the AF case, are not the future direction of housing development in China, settlement planning insights from this form can also enlighten the planning of future settlements.

6.2. Roofs in Urban Settlements Are Currently the Most Solar-Utilized Exterior Surfaces of Buildings, and with Economic Threshold Gradually Decreasing in the Future, Building Facades Have a Greater Potential for Solar Energy Utilization

The results of the year-by-year solar radiation simulations for 30 typical urban settlement models showed that rooftops had the highest average radiation levels, as well as power generation contribution to the distribution of solar radiation, of neighborhood build-

ing façades. Six neighborhood indicators were selected in this study, and two of the four indicators that showed strong correlations with the radiation data for power generation were the ratios of neighborhood roof area. This reveals the importance of building roof area in the development of solar resources. Again, taking the AF block as an example, it can be found that the highest total solar power generation is obtained by maximizing rooftop solar resource development, since the building density inside the site was only 50.6%.

From the analysis of the data, it is clear that the rooftop is the preferred location for solar energy development. In the settlement planning process, the percentage of building roof area in the settlement environment can be appropriately increased to obtain a higher level of solar power generation. From the comparison between the AF and A blocks, it can be found that the increase in building roof area in the AF block compared to the A block led to an increase in solar power generation per unit of land area up to 453.4%. Under the same building volume ratio, increasing the building roof area can significantly increase the solar energy development in the settlement.

The above analysis was performed under threshold control conditions, with the roof as the main location for solar resource development. Under natural radiation conditions, the building façades also have a high distribution of solar radiation according to the distribution of radiation data. Under threshold control conditions, more radiation on the façade could not meet the radiation utilization criteria and could not be developed. From the analysis in Section 4.5, it can be seen that the threshold standard changes with policy subsidies and equipment costs, and the threshold will be reduced in the future as the PV cost decreases and the conversion factor of PV systems increases. As a result, the building façades will have high utilization values and development potential in the future.

With the accelerated urbanization and economic development in China, urban housing is becoming larger and larger, and the number of available building roofs will increase. At the same time, technological progress has brought about a lower threshold standard, providing the possibility of using solar energy for residential façades. In summary, it can be suggested that in the future, the roofs and façades of buildings in urban settlements will provide a large development space for solar energy resource development. Newly built urban settlements can also improve the level of exploitable solar energy through targeted energy savings design.

Author Contributions: Conceptualization, J.L.; methodology, Z.L.; writing—review, and editing, Z.L. and Y.W.; supervision, project administration, and funding acquisition, H.Z. All authors have read and agreed to the published version of the manuscript.

Funding: This research is funded by National Natural Science Foundation of China (No. 52078265).

Informed Consent Statement: Informed consent was obtained from all subjects involved in the study.

Data Availability Statement: Data sharing is not applicable to this article as no new data were created or analyzed in this study.

Conflicts of Interest: The authors declare no conflict of interest.

References

1. Farooq, S.; Ozturk, I.; Majeed, M.T.; Akram, R. Globalization and CO₂ emissions in the presence of EKC: A global panel data analysis. *Gondwana Res.* **2022**, *106*, 367–378. [[CrossRef](#)]
2. Guesmi, K.; Makrychoriti, P.; Spyrou, S. The relationship between climate risk, climate policy uncertainty, and CO₂ emissions: Empirical evidence from the US. *J. Econ. Behav. Organ.* **2023**, *212*, 610–628. [[CrossRef](#)]
3. Guan, Y.; Xiao, Y.; Rong, B.; Kang, L.; Zhang, N.; Chu, C. Heterogeneity and typology of the city-level synergy between CO₂ emission, PM_{2.5}, and ozone pollution in China. *J. Clean. Prod.* **2023**, *405*, 136871. [[CrossRef](#)]
4. Parmesan, C.; Morecroft, M.D.; Trisurat, Y. *Climate Change 2022: Impacts, Adaptation and Vulnerability*; GIEC: Hong Kong, China, 2022.
5. Antonio, T. *The Energy Crisis in the World Today: Analysis of the World Energy Outlook 2021*; Johns Hopkins University: Baltimore, MD, USA; Universitat Pompeu Fabra: Barcelona, Spain, 2022.
6. Herzer, D. The impact on domestic CO₂ emissions of domestic government-funded clean energy R&D and of spillovers from foreign government-funded clean energy R&D. *Energy Policy* **2022**, *168*, 113126. [[CrossRef](#)]

7. Building-Integrated Photovoltaic Technologies and Systems for Large-Scale Market Deployment: The PV Sites Project. 2016. Available online: <http://www.pvsites.eu/> (accessed on 4 July 2023).
8. Home | MUSTEC. Available online: <https://mustec.eu/> (accessed on 4 July 2023).
9. Eranetmed—Era-Learn. Available online: <https://www.era-learn.eu/network-information/networks/eranetmed> (accessed on 4 July 2023).
10. National Development and Reform Commission. Notice of the “Fourteenth Five-Year Plan” Modern Energy System. Available online: https://www.ndrc.gov.cn/xxgk/zcfb/ghwb/202203/t20220322_1320016.html?code=&state=123 (accessed on 4 July 2023).
11. Nie, H.; Kemp, R.; Fan, Y. Investigating the adoption of energy-saving measures in residential sector: The contribution to carbon neutrality of China and Europe, Resources. *Conserv. Recycl.* **2023**, *190*, 106791. [[CrossRef](#)]
12. Mostafa, N.A.; Grida, M.; Park, J.; Ramadan, H.S. A sustainable user-centered application for residential energy consumption saving. *Sustain. Energy Technol. Assess.* **2022**, *53*, 102754. [[CrossRef](#)]
13. Zou, Y.; Deng, Y.; Xia, D.; Lou, S.; Yang, X.; Huang, Y.; Guo, J.; Zhong, Z. Comprehensive analysis on the energy resilience performance of urban residential sector in hot-humid area of China under climate change. *Sustain. Cities Soc.* **2023**, *88*, 104233. [[CrossRef](#)]
14. Mujeebu, M.A.; Bano, F. Energy-saving potential and cost-effectiveness of active energy-efficiency measures for residential building in warm-humid climate. *Energy Sustain. Dev.* **2022**, *67*, 163–176. [[CrossRef](#)]
15. Vargas, A.P.; Hamui, L. Thermal Energy Performance Simulation of a Residential Building Retrofitted with Passive Design Strategies: A Case Study in Mexico. *Sustainability* **2021**, *13*, 8064. [[CrossRef](#)]
16. Liu, S.; Kwok, Y.T.; Lau, K.K.-L.; Ouyang, W.; Ng, E. Effectiveness of passive design strategies in responding to future climate change for residential buildings in hot and humid Hong Kong. *Energy Build.* **2020**, *228*, 110469. [[CrossRef](#)]
17. Chi, F.; Wang, R.; Wang, Y. Integration of passive double-heating and double-cooling system into residential buildings (China) for energy saving. *Sol. Energy* **2021**, *225*, 1026–1047. [[CrossRef](#)]
18. Zhou, Z.; Wang, C.; Sun, X.; Gao, F.; Feng, W.; Zillante, G. Heating energy saving potential from building envelope design and operation optimization in residential buildings: A case study in northern China. *J. Clean. Prod.* **2018**, *174*, 413–423. [[CrossRef](#)]
19. Resch, E.; Bohne, R.A.; Kvamsdal, T.; Lohne, J. Impact of Urban Density and Building Height on Energy Use in Cities. *Energy Procedia* **2016**, *96*, 800–814. [[CrossRef](#)]
20. Shareef, S. The impact of urban morphology and building’s height diversity on energy consumption at urban scale. The case study of Dubai. *Buold. Environ.* **2021**, *194*, 107675. [[CrossRef](#)]
21. Shi, Y.; Yan, Z.; Li, C.; Li, C. Energy consumption and building layouts of public hospital buildings: A survey of 30 buildings in the cold region of China. *Sustain. Cities Soc.* **2021**, *74*, 103247. [[CrossRef](#)]
22. Ahmadian, E.; Sodagar, B.; Bingham, C.; Elnokaly, A.; Mills, G. Effect of urban built form and density on building energy performance in temperate climates. *Energy Build.* **2021**, *236*, 110762. [[CrossRef](#)]
23. Xie, X.; Sahin, O.; Luo, Z.; Yao, R. Impact of neighborhood-scale climate characteristics on building heating demand and night ventilation cooling potential. *Renew. Energy* **2020**, *150*, 943–956. [[CrossRef](#)]
24. Sarralde, J.J.; Quinn, D.J.; Wiesmann, D.; Steemers, K. Solar energy and urban morphology: Scenarios for increasing the renewable energy potential of neighborhoods in London. *Renew. Energy* **2015**, *73*, 10–17. [[CrossRef](#)]
25. Groppi, D.; de Santoli, L.; Cumo, F.; Garcia, D.A. A GIS-based model to assess buildings energy consumption and usable solar energy potential in urban areas. *Sustain. Cities Soc.* **2018**, *40*, 546–558. [[CrossRef](#)]
26. Chen, Z.; Yu, B.; Li, Y.; Wu, Q.; Wu, B.; Huang, Y.; Wu, S.; Yu, S.; Mao, W.; Zhao, F.; et al. Assessing the potential and utilization of solar energy at the building-scale in Shanghai. *Sustain. Cities Soc.* **2022**, *82*, 103917. [[CrossRef](#)]
27. An, Y.; Chen, T.; Shi, L.; Heng, C.K.; Fan, J. Solar energy potential using GIS-based urban residential environmental data: A case study of Shenzhen, China. *Sustain. Cities Soc.* **2023**, *93*, 104547. [[CrossRef](#)]
28. Yildirim, D.; Büyüksalih, G.; Şahin, A.D. Rooftop photovoltaic potential in Istanbul: Calculations based on LiDAR data, measurements and verifications. *Appl. Energy* **2021**, *304*, 117743. [[CrossRef](#)]
29. Kaleshwarwar, A.; Bahadure, S. Assessment of the solar energy potential of diverse urban built forms in Nagpur, India. *Sustain. Cities Soc.* **2023**, *96*, 104681. [[CrossRef](#)]
30. Li, J.; Wang, Y.; Xia, Y. A novel geometric parameter to evaluate the effects of block form on solar radiation towards sustainable urban design. *Sustain. Cities Soc.* **2022**, *84*, 104001. [[CrossRef](#)]
31. Morganti, M.; Salvati, A.; Coch, H.; Cecere, C. Urban morphology indicators for solar energy analysis. *Energy Procedia* **2017**, *134*, 807–814. [[CrossRef](#)]
32. Poon, K.H.; Kämpf, J.H.; Tay, S.E.R.; Wong, N.H.; Reindl, T.G. Parametric study of URBAN morphology on building solar energy potential in Singapore context. *Urban Clim.* **2020**, *33*, 100624. [[CrossRef](#)]
33. *JGJ134-2010*; Design Standard for Energy Efficiency of Residential Buildings in Hot Summer and Cold Winter Zone. China Architecture & Building Press: Beijing, China, 2010.
34. *GB 50797-2012*; Code for Design of Photovoltaic Power Station. Shanghai Electric Power Design Institute Co., Ltd.: Shanghai, China, 2012.
35. Kumar, M.; Kumar, A. Performance assessment and degradation analysis of solar photovoltaic technologies: A review. *Renew. Sustain. Energy Rev.* **2017**, *78*, 554–587. [[CrossRef](#)]

36. National Development and Reform Commission. *Notice on Relevant Matters Concerning the Feed-in Tariff Policy for Photovoltaic Power Generation in 2020*; National Development and Reform Commission: Beijing, China, 2020. Available online: <http://www.ndrc.gov.cn/> (accessed on 1 June 2020).
37. Perez, R.; Ineichen, P.; Seals, R.; Michalsky, J.; Stewart, R. Modeling daylight availability and irradiance components from direct and global irradiance. *Sol. Energy* **1990**, *44*, 271–289. [[CrossRef](#)]
38. Chen, Y.; Liang, X.; Hong, T.; Luo, X. Simulation and visualization of energy-related occupant behavior in office buildings. *Build. Simul.* **2017**, *10*, 785–798. [[CrossRef](#)]

Disclaimer/Publisher’s Note: The statements, opinions and data contained in all publications are solely those of the individual author(s) and contributor(s) and not of MDPI and/or the editor(s). MDPI and/or the editor(s) disclaim responsibility for any injury to people or property resulting from any ideas, methods, instructions or products referred to in the content.